

Magnetic properties of small $3d$ and $4d$ transition metal clusters: The role of a noncompact growth

F. Aguilera-Granja*

*Departamento de Física Teórica, Atómica y Óptica, Universidad de Valladolid, E-47011 Valladolid, Spain*J. M. Montejano-Carrizalez[†] and R. A. Guirado-López[‡]*Instituto de Física “Manuel Sandoval Vallarta,” Universidad Autónoma de San Luis Potosí,**Alvaro Obregón 64, 78000 San Luis Potosí, Mexico*

(Received 1 September 2005; revised manuscript received 11 January 2006; published 23 March 2006)

Within the framework of a self-consistent *spd* tight-binding Hamiltonian and *ab initio* pseudopotential techniques we study the magnetic properties of small Co_N , Ni_N , Rh_N , and Pd_N ($N=4-21$) clusters having noncompact structures. Following the recently reported existence of a nonicosahedral growth for small Rh clusters, as well as the predicted high stability of open (bipolar) structures for the late $3d$ and $4d$ 13-atom transition metal clusters, we consider different growth sequences based in the atomic capping of small half-octahedral and tetrahedral cluster units, which can be considered in general as precursors of the lowest energy configurations reported by Bae *et al.* [Phys. Rev. B **70**, 195413 (2004)] and Chang and Chou [Phys. Rev. Lett. **93**, 133401 (2004)]. On the one hand, for noncompact unrelaxed Co_N and Ni_N clusters, which are elements characterized by a large exchange regime, we obtain a slowly decreasing average magnetization $\langle\mu\rangle$ with increasing the size of the clusters. In addition, for a given cluster size, the value of $\langle\mu\rangle$ for different isomers has been found to be determined in general by the average coordination number of the structures, i.e., less (more) coordinated structures have high (low) magnetization states due to d band narrowing effects. On the other hand, for unrelaxed Rh_N and Pd_N structures, which are defined as weakly ferromagnetic systems, a complex decreasing oscillatory behavior is obtained with average magnetic moments per atom which are in general in reasonable agreement with the measured data. Interestingly, in the case of Rh_N clusters for $N\geq 15$, the suggested bipolarlike structures are characterized by values of $\langle\mu\rangle$ of the order of $0.05\mu_B/\text{atom}$, in clear disagreement with experiment, a result that could be interpreted as the beginning of a different structural growth sequence where clusters need to rearrange themselves towards different structures with higher magnetization states. As expected, fully relaxed clusters leads to the existence of atomic configurations with a complex nonuniform distribution of interatomic distances that reduces in general the value of $\langle\mu\rangle$. We conclude that the normally observed oscillatory magnetization data in cluster systems could be induced by a growth behavior in which cluster geometries flip-flop between low and high symmetry atomic arrays.

DOI: [10.1103/PhysRevB.73.115422](https://doi.org/10.1103/PhysRevB.73.115422)

PACS number(s): 75.75.+a, 31.15.Ew, 31.15.Ct

I. INTRODUCTION

The field of transition metal (TM) nanostructures has become one of the most important issues in nanotechnology due to possible important applications in electronic devices, magnetic recording, environmental processes, and so on.¹⁻⁸ As is well known, the characterization and control of their morphology and microstructure are necessary for a complete understanding of the observed macroscopic behavior and as a consequence, a wide variety of experimental techniques have been developed in order to produce high quality samples with specific electronic and structural properties.

In the case of TM clusters the amount of experimental work has been growing steadily. A wide variety of transition metal nanoparticles (with different sizes and morphologies) have been generated by laser vaporization techniques and their mass spectra, ionization potentials, magnetic moments, and reactivity towards small gaseous molecules have been measured. In the small size regime, both theoretical studies as well as gas adsorption experiments have concluded that icosahedral structures are the most favored atomic arrays.⁸ However, extensive density functional theory (DFT) calcula-

tions at different levels of approximation [e.g., discrete variational methods,⁹ pseudopotential techniques,¹⁰ and all-electron calculations, using both the local density approximation (LDA) as well as gradient-corrected functionals (GGA) for the exchange correlation term] have found that the average magnetic moment per atom of these high symmetry structures is always enhanced with respect to the experimental measurements. This is particularly evident in the case of Rh clusters where a value of $\langle\mu\rangle=1.6\mu_B/\text{atom}$ is obtained for the 13-atom icosahedral structure,¹⁰ which is considerably high when compared to the value of $0.48\pm 0.12\mu_B/\text{atom}$ measured by Cox *et al.*⁴ To explain these notable differences, several authors have underlined the need of including in the theoretical modeling the influence of possible isomerization effects,¹¹ the normally neglected orbital contributions to the total magnetization,¹² as well as an extensive sampling of all the possible spin multiplicities in the clusters. The latter is particularly important due to the well-known existence of several magnetic solutions to the Kohn-Sham equations that introduce some degree of uncertainty in the theoretical data.

Recently, Bae *et al.*¹³ have found a new possible source of discrepancy since they have obtained, for small Rh clusters, new low energy structures that are noncompact and have no atom in the center leading, in contrast to what was normally assumed, to a nonicosahedral growth. Furthermore, along the same line, Chang and Chou have found that, for the late 3*d* and 4*d* transition metal elements, 13-atom clusters are more stable in the form of a low symmetry biplanarlike structure.¹⁰ Here, it was concluded that this new low symmetry structure was stabilized by enhanced *s-d* hybridizations and, in addition, it was characterized by having magnetic moments smaller than those of an icosahedral array, being closer (but still higher) than the available experimental results.⁴ Finally, Xiao and Wang¹⁴ have recently reported that, in the case of Pt clusters up to 55 atoms, layeredlike structures are found to be as stable as their close-packed isomers. The previous reports strongly suggest that small transition metal clusters could exhibit a wide variety of complex growth sequences (different from the high symmetry structures normally proposed) that could be at the origin of the measured magnetization data due strong sensitivity of the spin-polarized charge distribution to the changes in the local atomic environment.

By looking at these new theoretically proposed low energy cluster structures we have found that, in general, they can be generated by considering an organized atomic capping of well-defined tetrahedral and half-octahedral subunits and, as a consequence, we have decided to perform in this work extensive self-consistent *spd* tight-binding (TB) and *ab initio* pseudopotential calculations on Co_N , Ni_N , Rh_N , and Pd_N clusters following various noncompact families of structures. Even if, in general, no effort will be made to explore the lowest energy atomic structure of all our considered clusters, i.e., we mainly report single-point TB electronic structure calculations on 3*d* and 4*d* transition metal clusters at their corresponding bulk interatomic distance, we believe that our results could be important since, in real systems, it is possible that during the growth sequence clusters might rearrange themselves around highly symmetric atomic arrays, passing through several intermediate transition structures such as the ones proposed in this work. Actually, only in the case of 13-atom clusters, we will perform additional calculations for representative structures at different interatomic distances as well as for fully relaxed structures in order to shed some light into the role played by relaxation effects. Finally, by performing a systematic comparison with experimental average magnetization measurements we will try to determine the extension of the different growth sequences in order to define critical cluster sizes at which possible structural transitions might take place. Of course, complex structural transitions between low and high symmetry structures could be present and surely will play a crucial role in the observed magnetic behavior.

The rest of the paper is organized as follows. In Sec. II we briefly described the theoretical models use for the calculations of the electronic, magnetic, and structural properties for our clusters. In Sec. III our results are discussed, and finally in Sec. IV our summary and conclusions are given.

II. THEORETICAL MODELS

Structural and electronic aspects have to be considered in the study of the magnetic properties of transition metal clus-

ters. Strictly speaking, calculations involving a simultaneous unconstrained relaxation of the geometry and unrestricted total spin value for the clusters are necessary. However, this type of calculations implies formidable computational requirements. Actually, for clusters containing more than seven atoms, the *ab initio* determinations of the ground-state structures become computationally difficult and, already for that range of sizes, it is common to combine different theoretical approaches to obtain first the ground-state structures within a simplified scheme (semiempirical potentials, absence of magnetic interactions, etc.), and then use a different methodology to analyze, by performing single-point calculations, the electronic and magnetic properties of the systems. In this paper we will use this kind of combined theoretical approach presenting first our TB results for the magnetic properties of unrelaxed clusters and then, by fully relaxing representative structures by means of nonspin-polarized pseudopotential DFT techniques, we will analyze the role played by complex structural relaxations in the average magnetization of the particles by performing single-point TB calculations on the previously optimized cluster arrays.

A. Tight-binding electronic Hamiltonian

The magnetic and electronic properties of our considered clusters are determined by solving a realistic *spd*-band tight-binding Hamiltonian including intra-atomic Coulomb interactions in the unrestricted Hartree-Fock approximation. In the usual notation it is given by

$$H = \sum_{i\alpha\sigma} \epsilon_{i\alpha\sigma} n_{i\alpha\sigma} + \sum_{\substack{i\alpha\sigma \\ i \neq j}} t_{ij}^{\alpha\beta} c_{i\alpha\sigma}^\dagger c_{j\beta\sigma}, \quad (1)$$

where $c_{i\alpha\sigma}^\dagger$ ($c_{j\beta\sigma}$) is the operator for the creation (annihilation) of an electron with spin σ at the orbital α (β) of atomic site i (j), and $n_{i\alpha\sigma}$ is the number operator. Electron delocalization within the system is described by the Slater-Koster hopping integrals $t_{ij}^{\alpha\beta}$, which were included up to the third nearest neighbors and assumed to be spin independent. The hopping integrals between neighboring orbitals are obtained from bulk-band structure calculations.¹⁵ Moreover, since we are using farther neighbor interactions r_{ij} , we assume that the hopping integrals obey the usual power law $(r_0/r_{ij})^{l+l'+1}$, where r_0 is the bulk nearest neighbor interatomic distance and l and l' are the orbital angular momenta of the orbital states involved in the hopping process.¹⁶

The spin- and environment-dependent energy levels $\epsilon_{i\alpha\sigma}$ in the Hamiltonian are given by

$$\epsilon_{i\alpha\sigma} = \epsilon_{i\alpha}^0 + z_\sigma \sum_\beta \frac{J_{\alpha\beta}}{2} \mu_{i\beta} + \Omega_{i\alpha}. \quad (2)$$

Here, $\epsilon_{i\alpha}^0$ refers to the orbital energy levels in the paramagnetic solution of the bulk. The second term is the correction for spin polarization of the electrons at site i ($\mu_{i\beta} = \langle n_{i\beta\uparrow} \rangle - \langle n_{i\beta\downarrow} \rangle$). In this second term, the $J_{\alpha\beta}$ are the exchange integrals and z_σ is the sign function ($z_\uparrow = +1$; $z_\downarrow = -1$). As usual, we neglect the exchange integrals involving *sp* electrons, taking into account only the integral corresponding to the *d*

electrons J_{dd} . Note that spin polarization of the delocalized sp band is also possible as a consequence of hybridization with the d states.

The exchange integrals for Co and Ni were fitted in order to reproduce the bulk magnetic moment¹⁷ (without orbital contribution) such as in our previous works for $3d$ clusters, being $J_{dd}(\text{Co})=1.44$ eV and $J_{dd}(\text{Ni})=1.234$ eV, respectively.^{18,19} In the case of Pd and Rh since both are paramagnetic in the bulk, the exchange parameter is obtained in such a way that we reproduce the value of the average magnetic moments of 13-atom Rh and Pd icosahedral clusters obtained by means of density functional theory (DFT) calculations.^{9,20,21} The values of the exchange parameters fitted in this way are $J_{dd}(\text{Rh})=0.40$ eV and $J_{dd}(\text{Pd})=0.60$ eV and have been already used in previous works.^{11,22} Finally, the site- and orbital-dependent potentials $\Omega_{i\alpha}$ are determined self-consistently in order to ensure that the sum of the s , p , and d electronic occupations satisfies the local charge neutrality condition.

The spin-dependent local electronic occupations are self-consistently obtained from the local density of states (LDOS), $\rho_{i\alpha\sigma}$, as

$$\langle \hat{n}_{i\alpha\sigma} \rangle = \int_{-\infty}^{\varepsilon_F} \rho_{i\alpha\sigma}(\varepsilon) d\varepsilon. \quad (3)$$

The LDOS are determined by calculating the Green's function $G_{i\alpha\sigma,i\alpha\sigma}(\varepsilon)$ [$\rho_{i\alpha\sigma}=(-1/\pi)\text{Im}\{G_{i\alpha\sigma,i\alpha\sigma}(\varepsilon)\}$] using the Haydock-Heine-Kelly recursion method.¹⁶ In this way, the distribution of the local magnetic moments ($\mu_i=\sum_{\alpha}\mu_{i\alpha}$) and the average magnetic moment per atom [$\langle\mu\rangle=(1/N)\sum_i\mu_i$] of the clusters are obtained at the end of the self-consistent cycle.

B. Pseudopotential approach

The structural properties of selected $3d$ and $4d$ cluster have been obtained, in the absence of magnetic interactions, within the DFT approach using the ultrasoft pseudopotential approximation for the electron-ion interaction and a plane wave basis set for the wave functions as implemented in the PWSCF code.²³ For all our considered structures, the cutoff energy for the plane wave expansion is taken to be 207 eV. A cubic supercell with a side dimension of 20 Å was employed in the calculations and the Γ point for the Brillouin zone integration. In all cases, we use the Perdew-Burke-Ernzerhof (PBE) exchange-correlation potential which has nonlinear core corrections and a semicore state d in the valence region. We perform nonspin-polarized structural optimizations for selected clusters without any symmetry constraints using the conjugate gradient method. The total energy is converged to 10^{-4} eV in the self-consistent process and the force on each atom is always less than 0.02 eV/Å in all our equilibrium configurations.

At this point, it is important to comment that including the existence of local magnetic moments in the minimization process normally yields cluster structures with slightly expanded interatomic distances when compared with the nonmagnetic solution. This expansion is particularly pronounced

in particles having very large local magnetizations which cause the repulsive magnetic force $F_{\text{mag}}=\partial\Delta E_m/\partial r$, where $\Delta E_m=E(\mu=0)-E(\mu)$ is the magnetic energy gain, to be particularly large. Actually, in small Cr_N clusters which have local magnetic moments in the range of 4.7–5.0 μ_B , even an expansion with respect to the bulk interatomic spacing has been obtained.²⁴ Here, as we will see in the following, with the exception of a few very small Co clusters, we will be dealing in general with structures having a local moment distribution that varies in the range of 0.1–2.0 μ_B and we expect thus that this effect will not be of crucial importance in determining the lowest energy atomic array.

III. RESULTS AND DISCUSSION

In this section we describe the precise geometrical details of our considered growth sequences as well as the magnetic properties obtained for unrelaxed Co_N , Ni_N , Rh_N , and Pd_N clusters following the previously defined various families of structures. While in the case of Co_N and Ni_N clusters a slowly decreasing average magnetization as a function of the cluster size is always found, we will show that, for Rh_N and Pd_N clusters, a strong oscillatory behavior is obtained in all the growth modes due to the strong sensitivity of the spin-polarized charge distribution to the precise details of the local atomic environment. Finally, for some representative 13-atom clusters, we will present additional TB magnetic calculations by assuming uniform contractions of the interatomic bond lengths as well as by fully relaxing the cluster structures by means of *ab initio* pseudopotential techniques.

A. Cluster geometries

Different noncompact growth sequences can be generated by using different initial seed clusters. In general in our work, three (or four) coordinated sites in our seed clusters are selectively capped, forming in this way well-defined tetrahedral (or half-octahedral) subunits. Depending on the considered seed cluster and initial capping, different growth families or sequences are obtained, such as the ones illustrated in Figs. 1–3. In all the figures, the gray circles define different base clusters on which additional atoms (dark circles) can be placed in several positions defining our considered different growth sequences. In particular, the family of structures shown in Fig. 1 is the one that includes the biplanarlike cluster recently proposed by Chang and Chou¹⁰ [see Fig. 1(e)]. In this growth sequence, the initial seed cluster [see Fig. 1(a)] is the square pyramid (half-octahedral) unit. In the case of $N=13$ we consider two possibilities, as shown in Figs. 1(e) and 1(f), where the former corresponds to the structure proposed in Ref. 10 and the latter is an alternative cluster constructed by simply assuming a different disposition of the two new atoms added to the 11-atom structure shown in Fig. 1(d). Finally, it is important to comment that the cluster geometries shown in Figs. 1(g) and 1(h) define two of the possible growth paths that can be constructed from the biplanar cluster proposed by Chang and Chou, whereas Fig. 1(i) is a biplanar structure based on the cluster shown in Fig. 1(h). We define this biplanar growth mode as sequence 1 ($S1$).

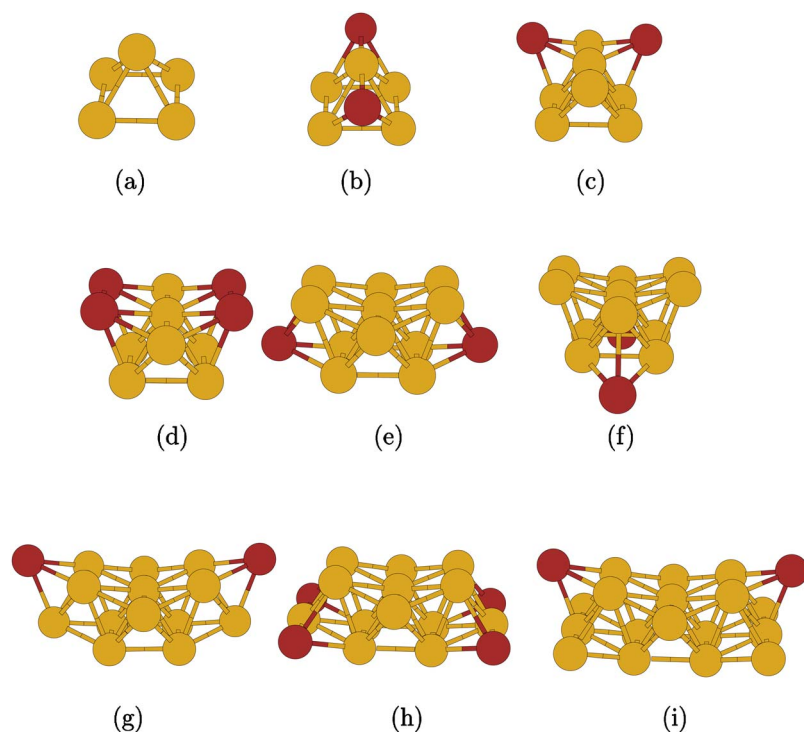


FIG. 1. (Color online) Growth sequence based on the half octahedral seed structure shown in (a). The gray circles define in each case the core cluster in which additional atoms (dark circles) can be placed in different positions. The structure shown in (e) corresponds to the biplanar structure proposed by Chang and Chou (Ref. 10). We call this growth mode sequence 1 ($S1$).

In Fig. 2, we present an alternative growth path based on the same seed cluster shown in Fig. 1(a). Notice that the structures shown in Figs. 2(a) and 2(b) are common to the cluster growth of Fig. 1. However, Figs. 2(c)–2(g) define a kind of layered growth with local fivefold symmetry at the center of the clusters. We define this family of structures as sequence 2 ($S2$). Notice that the clusters shown in Figs. 2(a)–2(e), 2(h), and 2(i) represent an alternative biplanar growth different from the one proposed in $S1$. We call this growth mode sequence 3 ($S3$).

Finally, in Fig. 3 we show the icosahedral family of structures which is constructed from the capping of a tetrahedral seed cluster [see Fig. 3(a)]. We call this family ICO sequence. Notice that in Fig. 3(e) we have changed the orientation of the previous cluster shown in Fig. 3(d) in order to make more clear the disposition of the atoms in the structure. It is important to comment that, in all our considered clusters shown in Figs. 1–3, all the nearest neighbor interatomic distances are always fixed to the corresponding bulk value. However, for some particular cases, we will also consider structures with both uniform contractions and fully relaxed interatomic distances in order to analyze the role played by bond length changes in the cluster average magnetization. Even if it is clear that our theoretical procedure does not allow us to determine the global minimum, we believe that we will provide the magnetic properties of stable, and still unexplored, low energy configurations that could be present in the experiments.

B. Magnetic properties of $3d$ Co_N and Ni_N clusters

In Fig. 4, we present the average spin magnetic moment for unrelaxed Ni_N and Co_N clusters (which are elements characterized by a large exchange regime) calculated by Hamiltonian (1) for all the growth sequences shown in Figs. 1–3.

We always compare with available experimental measurements as well as first-principles calculations which will serve as a critical justification of our TB parametrization scheme. From Figs. 4(a) and 4(b) we notice that in the case of $3d$ Ni_N and Co_N clusters, despite the low symmetry of the different growth sequences and the rapidly changing local atomic environment (see Figs. 1–3), a slowly decreasing average magnetization as a function of the cluster size is always obtained. As is well known, in general the magnetization state of a magnetic cluster is a result of a very complex process involving a delicate interplay among electronic and geometrical factors, however, we have noted that in the case of small Ni_N and Co_N clusters, the observed trends can be most often understood by following the well-known correlation between magnetism and the local coordination number of the structures, namely, less coordinated atoms have enhanced magnetic moments when compared to the more coordinated sites due to d band narrowing effects.

When comparing with the experimental magnetization measurements for Ni_N clusters performed by Apsel *et al.*,⁵ we observe from Fig. 4(a) that our calculated values for the different growth sequences are located more or less around the measured data, with the exception of values of N around 13 where there is a significant drop in the experimental data, and it is not possible to infer, based on the direct comparison, the actual cluster structures synthesized in Apsel's experimental work. However, from the figure we clearly notice that for $N=19$ the icosahedral array yields more reduced values of $\langle \mu \rangle$ when compared with the measured magnetic moments, and that all the low symmetry biplanarlike structures ($S1$, $S2$, and $S3$) are the ones having average magnetizations in better agreement with experiments. Finally, it is important to notice that within our theoretical framework, the unrelaxed 13-atom biplanarlike structure shown in Fig. 1(e) is characterized (as the rest of the 13-atom isomers) by a value

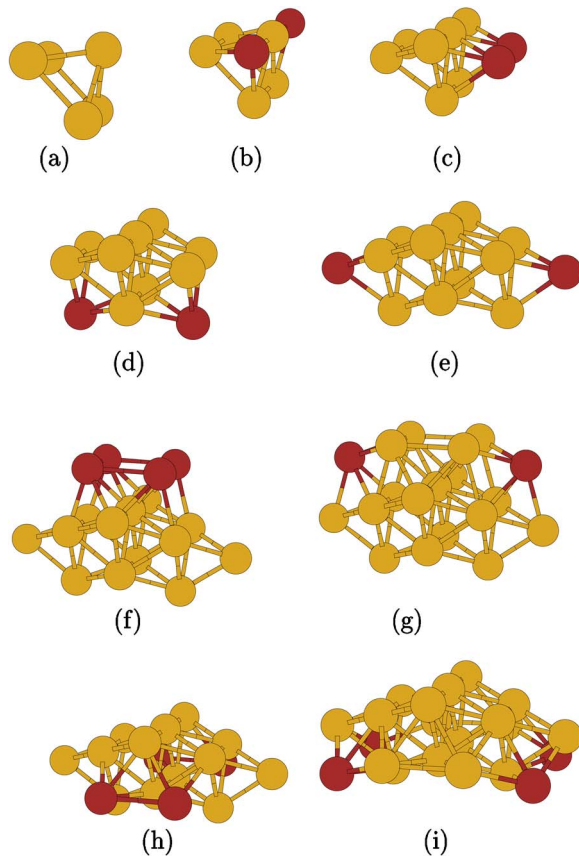


FIG. 2. (Color online) Same as in Fig. 1 but where the nine-atom isomer shown in (c) is formed now by adding two new atoms to the seven-atom structure shown in (b) on the pair of neighboring triangular faces [compare with Fig. 1(c)]. The cluster sequence illustrated in (a)–(g) corresponds to a layered growth, defined as sequence 2 (S2), while the configurations shown in (a)–(e), together with the structures shown in (h) and (i), correspond to a different biplanarlike growth defined as sequence 3 (S3).

for $\langle\mu\rangle$ which is $\sim 0.4 \mu_B/\text{atom}$ higher than the one reported in the experiments of Apsel and co-workers.⁵ This result is worth noticing since, in the work of Chang and Chou,¹⁰ it was predicted that the high stability of the open 13-atom biplanar structure with respect to the icosahedral array must be expected to hold also for the late $3d$ TM clusters. However, from the figure it is clear that, from the point of view of its magnetic properties, this noncompact structure has an average magnetization very different from the one observed in the measured data.

Of course we must say that, in the case of Ni_N clusters, there could be some other factors at the origin of the notable differences obtained between theory and experiment. First, our magnetization data must be accompanied by a geometry unrestricted optimization calculation in order to better define, for each N , the corresponding lowest energy atomic configuration. Second, it is important to say that for a given size, various isomers (as the ones considered in the present work) could be simultaneously present in the experimental setup and as a consequence the measured data could be also interpreted as complex mixture of the average magnetization of various cluster structures (so-called isomerization effects).

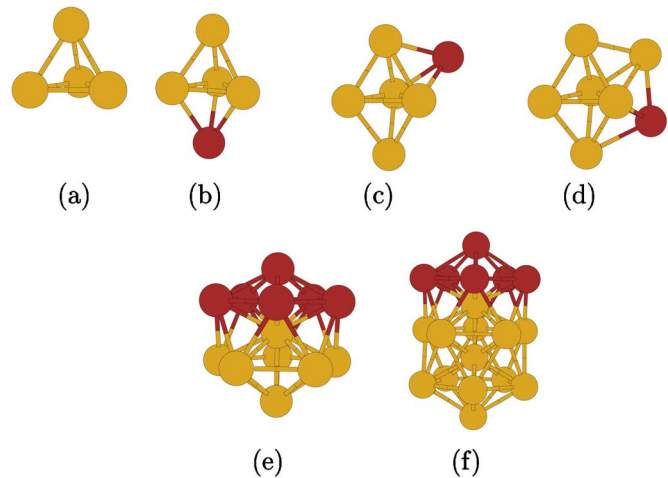


FIG. 3. (Color online) The icosahedral like family of structures which is based on the capping of the tetrahedral seed cluster shown in (a). We call this growth mode the ICO sequence.

Finally, the orbital contribution L to the cluster total magnetization M ($M=2S+L$) has been already shown to be important¹² and actually, for the cluster sizes considered in Fig. 4(a), the values of L have been found to be approximately in the range of $0.18\text{--}0.48 \mu_B$, values which are expected to result in a more realistic comparison with the experiments.

At this point, it is important to comment that our considered biplanar configurations shown in Figs. 1 and 2 are idealized in the sense that all its Ni-Ni bonds have equal values, being fixed to the fcc Ni bulk interatomic spacing (2.5 \AA). However, it is clear that the different forces acting on atoms having different local atomic environments are expected to induce a nonuniform distribution of contracted Ni-Ni bond lengths within the structures, which will lower the symmetry of the clusters and could reduce our calculated average magnetization $\langle\mu\rangle$. In order to explore thus the role played by this kind of structural transformations, we have performed first uniform contractions for the cluster structures shown in Fig. 1(e) and Fig. 3(e). Of course, these types of distance variations can induce energy level inversions around the Fermi energy of the systems a fact that, in some cases, could strongly change the spin-polarized electronic occupations and reduce the average magnetization of the clusters. Furthermore, the low symmetry of the biplanar structures is expected to favor the existence of these energy level inversions since a low degenerated and closely spaced electronic spectra is expected to characterize this type of cluster arrays.

In Fig. 5 we plot the behavior of the average magnetic moment per atom as a function of the degree of contraction of the interatomic distance for both biplanar [Fig. 1(e)] and icosahedral [Fig. 3(e)] structures. From Fig. 5 we can see that, as the bond length is reduced, the value for $\langle\mu\rangle$ decreases in both types of structures due to the increase d - d hybridization and enhanced electron delocalization in the structures. Notice that, as already commented above, the less symmetric biplanar array presents a more continuous variation of $\langle\mu\rangle$ when the interatomic distance is reduced since it is characterized by a closely spaced electronic spectra around

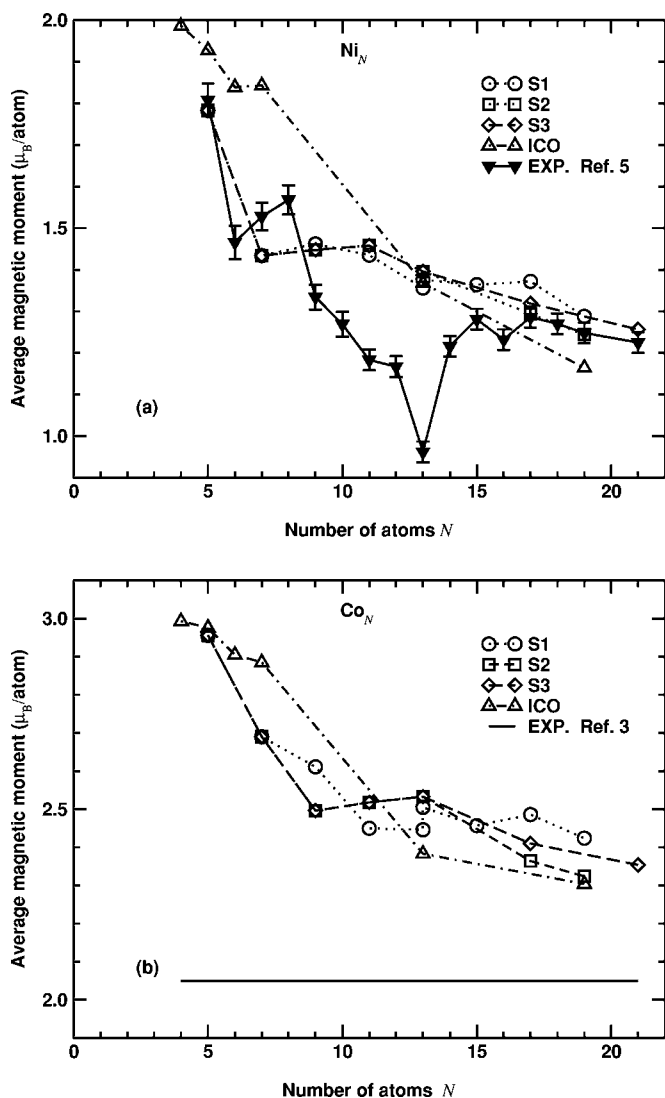


FIG. 4. The calculated average magnetic moment (in units of μ_B/atom) as a function of the number of atoms N for (a) Ni_N and (b) Co_N clusters assuming the different growth sequences shown in Figs. 1–3. The experimental data for Ni and Co clusters obtained from Refs. 5 and 3, respectively, are also shown.

the Fermi energy, a fact that leads to a more easier destabilization of the magnetic solutions when R/R_b is reduced. In contrast, for the more symmetric icosahedral array, characterized by a highly degenerated and more largely spaced energy level distribution, we can clearly appreciate the presence of well defined region of R/R_b having constant values of $\langle \mu \rangle$, which implies the existence of highly stable magnetic states. However, it is important to remark that within our theoretical approach, reasonable contractions of the interatomic spacing (up to 10% of reduction with respect to the bulk value) still yield enhanced values of $\langle \mu \rangle$ when compared with the experimental data [see Fig. 4(a)].

We show as insets in Fig. 5, the fully optimized structures for the icosahedral and biplanar arrays considered in the calculations by means of *ab initio* pseudopotential techniques. As expected, we notice that the icosahedral cluster preserves its original symmetry after the relaxation process, while the

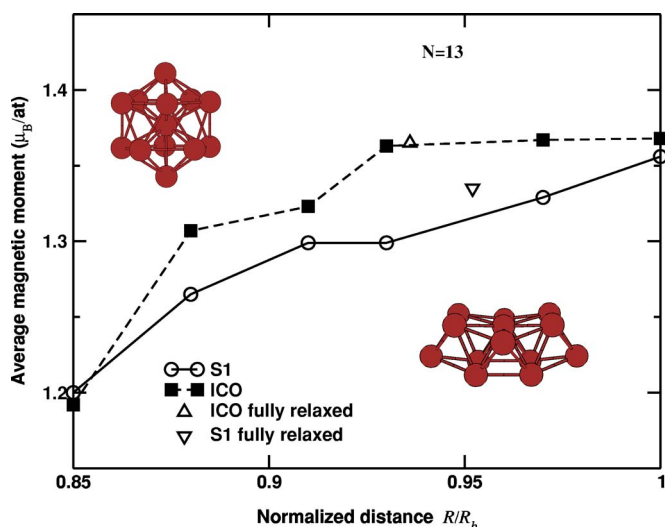


FIG. 5. (Color online) The calculated average magnetic moment (in units of μ_B/atom) for a Ni_{13} cluster adopting the biplanar [Fig. 1(e)] and ICO [Fig. 3(e)] structures as a function of the normalized interatomic distance R/R_b (R_b being the bulk value). As insets, we show also the fully optimized atomic configurations.

biplanar array is slightly bent since now the atoms forming each layer are not exactly on the same plane. In the former structure, even if an unconstrained optimization is performed, we have found that the final configuration obtained is equivalent to performing a uniform relaxation of the cluster lattice with a value of R/R_b of 0.94. However, for the latter low symmetry biplanar array, a complex distribution of contracted distances is found, ranging from 2.32–2.49 Å, being in average equivalent to a 5% of reduction. Finally in the figure, and as isolated empty up and down triangles, we include also the TB values of $\langle \mu \rangle$ for both icosahedral and biplanar fully relaxed atomic configurations, respectively. Interestingly, we see that the values of the average magnetization are located very closed to the $\langle \mu \rangle$ vs R/R_b curves and imply that, despite the low symmetry of the fully relaxed clusters, the magnetic properties of these species characterized by a large exchange regime could be inferred from those of uniformly contracted structures.

Finally, it is important to remark that the existence of a more stable structure (different from the ones considered in the present and previous works) could be also at the origin of the observed differences between theory and experiment in Fig. 4(a). This fact has been already seen in the case of Rh clusters where similar pseudopotential calculations performed recently by Bae *et al.*¹³ and Chang and Chou¹⁰ have predicted different lowest energy atomic configurations for the 13-atom structure. However, from our pseudopotential calculations we have found that, at least for nonmagnetic structures, the icosahedral array is still more stable by 0.44 eV. Consequently, a more extensive sampling of the configurational phase space would be required in order to more accurately established the lowest energy cluster array leading to the experimentally obtained average magnetization.

In Fig. 4(b), we show the values of $\langle \mu \rangle$ as a function of cluster size N for Co clusters ranging from Co_4 to Co_{21} , and

from which we can appreciate the same trends discussed in the previous paragraphs. When compared with the value obtained in the bulk hcp-phase ($1.7 \mu_B/\text{atom}$), we note a sizable enhancement of the average magnetization in all our considered structures. In all the growth sequences, $\langle \mu \rangle$ slowly decreases as a function of N , being again in general the structures with the lowest coordination number the ones having the largest values for the average magnetization. From the figure, it is important to notice that our calculated value for our biggest considered structure (21-atom cluster) is still overestimated when compared to the value obtained by Bilas *et al.*³ for their smallest considered Co cluster, which is of the order of ~ 43 atoms. This is in agreement with the well-known slow convergence of $\langle \mu \rangle$ to the bulk value also observed for Fe and Ni clusters. On the other hand, from the point of view of theory, our calculated average magnetization (as well as local site distribution) for the 13-atom Co icosahedral array ($2.38 \mu_B/\text{atom}$) is in good agreement with the value of $2.33 \mu_B/\text{atom}$ obtained by Li and Gu for the same unrelaxed icosahedral structure within the framework of DFT theory.²⁵ Furthermore, Miura *et al.*²⁶ have obtained a value of $2.23 \mu_B/\text{atom}$ for the icosahedral array by using the discrete variational X_α cluster method in good agreement also with our theoretical data. Finally, it is important to mention that there are some semiempirical TB calculations by Guevara *et al.*²⁷ and Andriotis and Menon²⁸ addressing the magnetic properties of small Co clusters. In the former case, the authors restricted their analysis to an fcc growth mode and it is thus not possible to compare their results with our average magnetization data. In the latter, the TB molecular dynamics relaxation procedure used by the authors led to unusual structural relaxations in which considerable expansions of the clusters lattice were obtained and, as a consequence, the calculated magnetic properties might not be very accurate. However, we believe that the previous comparisons with more accurate DFT methodologies are consistent and give us confidence in our considered parametrization setup.

C. Magnetic properties of $4d$ Rh_N and Pd_N clusters

In Figs. 6 and 7, we present the average spin magnetic moment per atom for unrelaxed $4d$ Rh_N and Pd_N clusters for all the growth sequences shown in Figs. 1–3. In the figures we also include the experimental average magnetization data obtained from Ref. 4 for Rh particles up to 21 atoms [Fig. 6(a)], together with the upper limit ($\sim 0.4 \mu_B/\text{atom}$) estimated for Pd clusters with sizes of the order of 13 atoms (Fig. 7). From both figures we can see that, in remarkable contrast to Ni and Co clusters [compare with Figs. 4(a) and 4(b)], for Rh and Pd clusters, a complex decreasing oscillatory behavior of $\langle \mu \rangle$ as a function of N is now obtained. As is well known, both Rh and Pd clusters are defined as weakly ferromagnetic systems and, as a consequence, the spin-polarized charge distribution is very sensitive to the precise details of the local atomic environment. Actually, this is what we observe in both Figs. 6(a) and 7 where the average magnetization changes drastically even when the cluster size is varied by a few atoms. It is thus clear that in these cases, the cluster geometry, the interatomic distance, and the precise details of the local atomic environment play a crucial role

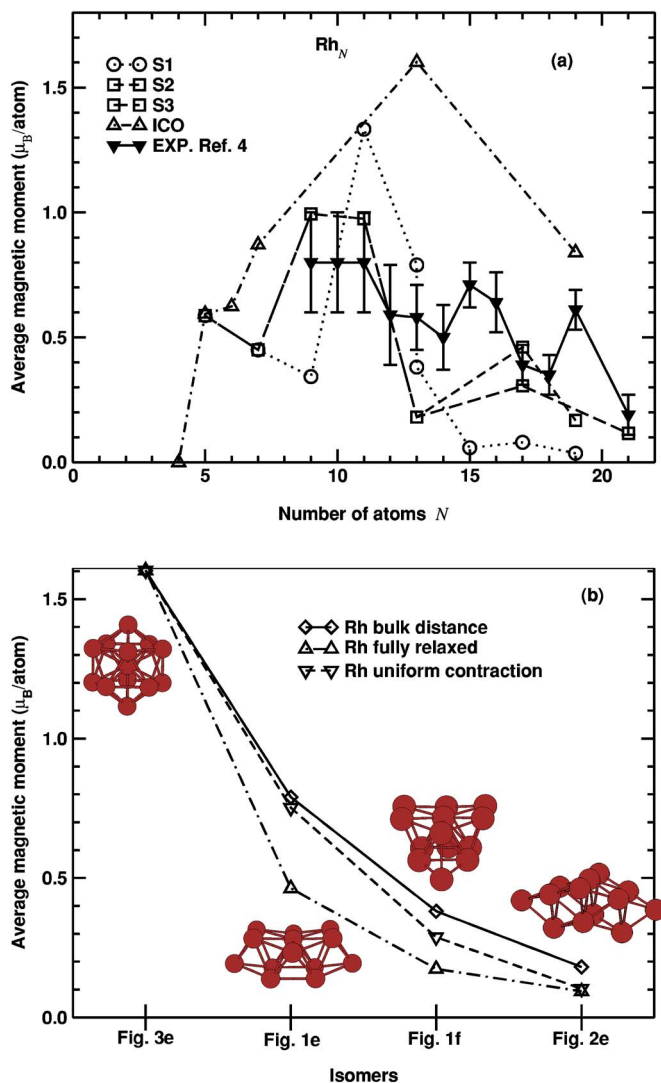


FIG. 6. (Color online) (a) The calculated average magnetic moment (in units of μ_B/atom) as a function of the number of atoms N for Rh_N clusters assuming the different growth sequences shown in Figs. 1–3. The experimental data for Rh clusters obtained from Ref. 4 are also shown. (b) The value of $\langle \mu \rangle$ for our considered 13-atom cluster isomers at the bulk interatomic distance, fully relaxed, and by performing a uniform contraction of the cluster lattice. We show also the fully optimized atomic configurations as insets.

into the understanding the complex magnetic behavior observed in the $4d$ elements.^{10,11,13,22,29}

In the case of Rh clusters [Fig. 6(a)] we can see that, in general, the values of $\langle \mu \rangle$ for the icosahedral fragments, which were considered to be the most stable arrays in earlier studies, are characterized by average magnetizations that are always overestimated with respect to the experimental measurements. Furthermore, with the inclusion of the (additive) orbital contributions to the cluster total magnetization, the observed discrepancy between theory and experiment is expected to become more pronounced. As a consequence, based on the previous direct comparison, it could be established that icosahedral configurations for small Rh clusters cannot be used to explain, at least in the small size regime, the observed trends in Cox *et al.*'s experimental results.⁴ In

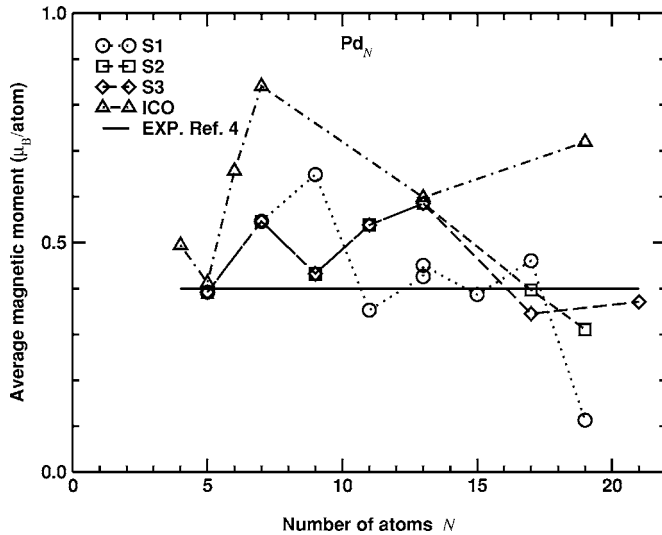


FIG. 7. The calculated average magnetic moment (in units of μ_B/atom) as a function of the number of atoms N for Pd_N clusters assuming the different growth sequences shown in Figs. 1–3. The experimental data for Pd clusters obtained from Ref. 4 are also shown.

contrast for the low symmetry layered structures [see Figs. 1 and 2], we notice that the values of $\langle\mu\rangle$ approximately oscillate around the measured data. In particular, in the case of our 13-atom clusters notice that, in agreement with the pseudopotential calculations of Ref. 10, the biplanarlike configuration shown in Fig. 1(e) is the one that has a value of $\langle\mu\rangle$ very close (although underestimated) to the experimental result.

At this point, it is important to comment that, previous calculations of the orbital contributions of the orbital magnetization L in small Rh clusters having different symmetries³⁰ have revealed that the local value of L can be as large as $0.4 \mu_B$ and, as a consequence, the total magnetization defined as $\langle M \rangle = 2\langle S \rangle + \langle L \rangle$ of the biplanarlike configuration is expected to more accurately match the experimental data. In contrast, for $N > 13$, we have found that the cluster structures following the S1 family are characterized by values of $\langle\mu\rangle$ of the order of $0.05 \mu_B/\text{atom}$, in clear disagreement with experiment, a result which could imply that clusters need to rearrange themselves towards different structures with higher magnetization states. Actually, for $N > 13$ we see that now the layered clusters belonging to the S2 and S3 families are the ones being closer to the experimental data. Consequently, the discrepancy seen in the experimental and theoretical results could be understood if a growth behavior in which cluster geometries flip-flop between low and high symmetry arrays is assumed.

It is important to comment also that in these type of clusters characterized by nonsaturated magnetism, structural relaxation effects could play an important role since, as has been already shown in Fig. 5, bond length variations could lead to important changes in the electronic structure with significant consequences for the magnetic behavior. Consequently, in Fig. 6(b) we show a systematic comparison of the values of $\langle\mu\rangle$ obtained for our considered 13-atom Rh iso-

mers at (i) the bulk-Rh interatomic distance, (ii) fully relaxed within the pseudopotential approach, and (iii) by assuming uniform contractions equivalent to the average relaxation obtained from (ii). From the insets of the figure, where we show the fully optimized structures, we can appreciate that, in all cases, the symmetry of the initially proposed seed clusters is still preserved after the relaxation process, which implies that these atomic configurations define low energy atomic arrays of the configurational phase space. Actually, the average contractions obtained for the icosahedral array and the biplanar structure [shown in Fig. 1(e)] which are of the order of 2.66 and 2.60 Å, respectively, are practically the same than the ones reported by Chang and Chou *et al.* which are equal to 2.67 and 2.60 Å. On the other hand, concerning the relative stability between the considered isomers we would like to comment that, in our nonmagnetic case, the icosahedral cluster is the most stable array; however, it is only 0.06 eV lower in energy than the biplanar configuration shown in Fig. 1(e). On the other hand, the structures corresponding to the S2 and S3 families are 0.84 and 0.35 eV less stable. We can conclude thus, by combining our theoretical data with the results of Ref. 10 that the energy gain obtained by allowing the existence of local magnetic moments in the clusters seems to be considerably larger in the biplanar configuration, a fact that could be enough to change the energy ordering between the icosahedral and biplanar isomers.

From Fig. 6(b) it is clearly seen that now, in contrast to Ni_N clusters, there are some cases in which notable differences in the values of $\langle\mu\rangle$ (calculated within the TB scheme) between unrelaxed structures and fully (or partially) optimized atomic arrays are obtained. This is particularly the case for the biplanar configuration shown in Fig. 1(e) where the globally optimized array has a value of $\langle\mu\rangle$ that is $\sim 0.3 \mu_B/\text{atom}$ smaller than both unrelaxed and uniformly contracted clusters, but actually in better agreement with experiment ($0.48 \pm 12 \mu_B/\text{atom}$). On the contrary, for the icosahedral and S3 structures we can appreciate that the calculated values of $\langle\mu\rangle$ for uniform relaxations of the cluster lattice are consistent with the values obtained in the fully relaxed configurations. However, it is important to comment that these structurally induced differences are expected to become less important with increasing N since bond length contractions will be less pronounced and, as a consequence, we believe that our $\langle\mu\rangle$ vs N curve shown in Fig. 6(a) should be more realistic for that range of sizes.

In Fig. 7, we show the calculated values of $\langle\mu\rangle$ for small unrelaxed Pd clusters adopting the structures shown in Figs. 1–3. As in the case of Rh clusters, we notice that the icosahedral arrays are characterized by having in general the largest values of $\langle\mu\rangle$. On the contrary, all low symmetry layered structures have values of $\langle\mu\rangle$ that oscillate around the estimated upper limit for clusters having sizes around 12 atoms. It is clear that in nonsaturated magnetic clusters a good geometrical structure is therefore crucial in order to correctly interpret the experimental measurements. Finally, when comparing our calculated values of $\langle\mu\rangle$ for the Pd_{13} clusters shown in Figs. 1(e) and 3(e), which are of the order of 0.42 and $0.6 \mu_B/\text{atom}$ respectively, with the values obtained in the pseudopotential calculations of Ref. 10 we can see that both

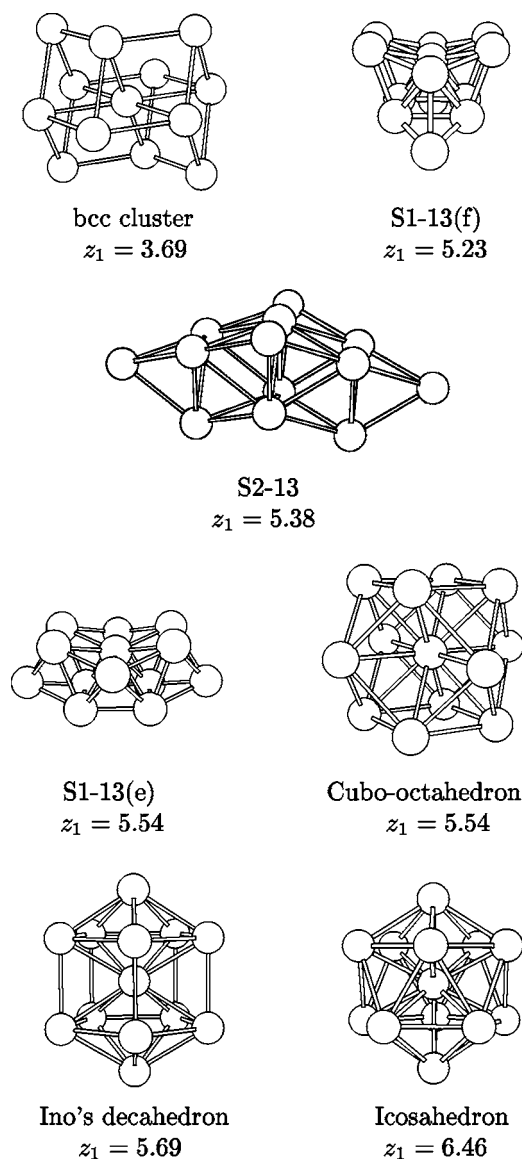


FIG. 8. Atomic configurations of the most common 13-atom transition metal clusters considered in the literature.

types of calculations are in reasonable agreement, a fact that give us confidence in our parametrization setup.

Finally, it is interesting to compare the magnetic properties of the most common 13-atom cluster isomers reported in the literature^{11,13,18–21,27,28,31,32} and that we show in Fig. 8. To simplify the comparison we plot in Fig. 9 the average magnetic moment per atom as a function of the effective coordination number z_{eff} of each one of the structures. We define $z_{eff} = z_1 + z_2/r_2^5$, where z_2 is the average number of next nearest neighbors atoms and r_2 corresponds to the next nearest neighbor distance. This effective coordination number allows us to distinguish between those structures with the same number of first nearest neighbors, and tells us which one is more compact.

From Fig. 9, we can see that, in general, there is a clear correlation between $\langle \mu \rangle$ and the effective coordination number z_{eff} of the structures. Notice that in the case of Ni_{13} and Co_{13} clusters an almost perfect linear dependence of $\langle \mu \rangle$ vs

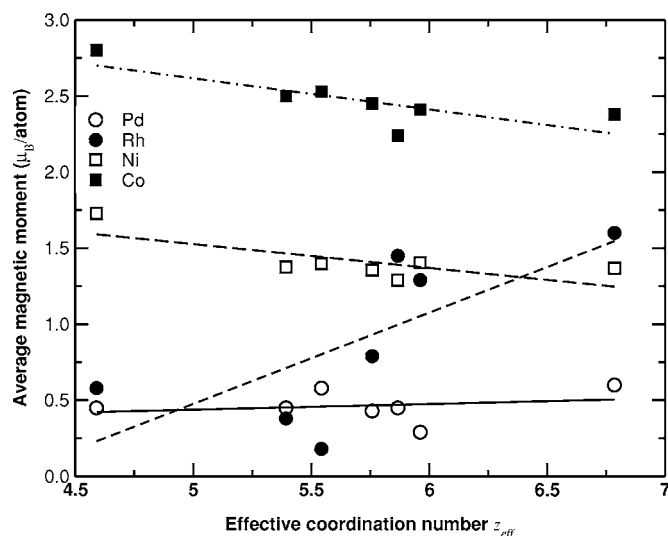


FIG. 9. The calculated average magnetic moment (in units of μ_B/atom) as a function of the effective coordination number z_{eff} for the different 13-atom clusters shown in Fig. 8. The straight lines are just a guide to the eye.

z_{eff} is obtained, while for Rh_{13} and Pd_{13} structures clear deviations from this simple dependence are found. Furthermore, we notice in the 3d clusters that the magnetic behavior can be also related to d -band filling effects since small Co clusters have values of $\langle \mu \rangle$ which are always enhanced with respect to the ones obtained in Ni_N structures, due to the larger number of holes (reduced number of d electrons) that can be polarized. Interestingly, for Rh and Pd clusters the previous criteria is not always satisfied. Consequently, considering that we are taking into account (at least partially) the environmental effects in the definition of z_{eff} , this allow us to say that, as already inferred from Figs. 4–7, in nonsaturated magnetic systems the electronic contributions are the ones that dominate over the local coordination number effects and produce the strong dispersion in the values of the average magnetic moments that deviate from the simply linear behavior.

IV. CONCLUSIONS

In this work we have presented a systematic theoretical study of the magnetic properties of small and unrelaxed Co_N , Ni_N , Rh_N , and Pd_N ($N=4–21$) clusters having noncompact structures by using a self-consistent spd tight-binding Hamiltonian within the unrestricted Hartree-Fock approximation as well as *ab initio* pseudopotential techniques. For the geometrical structures we have considered different growth sequences based in the atomic capping of small half-octahedral and tetrahedral cluster units, which can be considered in general as precursors of the lowest energy configurations recently reported by Chang and Chou¹⁰ as well as Bae and co-workers.¹³ We have found that, for noncompact Co_N and Ni_N clusters, which are elements characterized by a large exchange regime, a slowly decreasing average magnetization $\langle \mu \rangle$ with increasing the size of the clusters is obtained while, for Rh_N and Pd_N structures, a complex decreasing oscillatory

behavior is observed. Although in some cases the average magnetization of our considered layered structures reasonably agrees with the experimental results, we conclude that the general discrepancy seen between experimental and theoretical results could be also understood if a growth behavior in which cluster geometries flip-flop between low and high symmetry arrays is assumed.

ACKNOWLEDGMENTS

The authors would like to acknowledge the financial support from PROMEP-SEP/CA230 and (R.A.G.-L.) CONACyT/45928-E. F.A.-G. also acknowledges financial support from the Ministerio de Educación y Ciencia (Spain), Grant No. SAB2004-0129.

*Electronic address: faustino@ifisica.uaslp.mx

†Electronic address: jmme@ifisica.uaslp.mx

‡Electronic address: guirado@ifisica.uaslp.mx

- ¹J. P. Bucher and L. A. Bloomfield, *Int. J. Mod. Phys. B* **7**, 1079 (1993).
- ²J. A. Alonso, *Chem. Rev. (Washington, D.C.)* **100**, 637 (2000).
- ³I. M. L. Billas, J. A. Becker, A. Chatelain, and W. A. de Heer, *Phys. Rev. Lett.* **71**, 4067 (1993).
- ⁴A. J. Cox, J. G. Louderbak, S. E. Apsel, and L. A. Bloomfield, *Phys. Rev. B* **49**, 12295 (1994).
- ⁵S. E. Apsel, J. W. Emmert, J. Deng, and L. A. Bloomfield, *Phys. Rev. Lett.* **76**, 1441 (1996).
- ⁶T. Shinohara, T. Sato, and T. Taniyama, *Phys. Rev. Lett.* **91**, 197201 (2003).
- ⁷B. Sampedro, P. Crespo, A. Hernando, R. Litrán, J. C. Sánchez-López, C. López-Cartes, A. Fernandez, J. Ramírez, J. González-Calbet, and M. Válet, *Phys. Rev. Lett.* **91**, 237203 (2003).
- ⁸E. K. Parks, L. Zhu, J. Ho, and S. J. Riley, *J. Chem. Phys.* **100**, 7206 (1994); E. K. Parks and S. J. Riley, *Z. Phys. D: At., Mol. Clusters* **33**, 59 (1995).
- ⁹Yang Jinglong, F. Toigo, and W. Kelin, *Phys. Rev. B* **50**, 7915 (1994).
- ¹⁰C. M. Chang and M. Y. Chou, *Phys. Rev. Lett.* **93**, 133401 (2004).
- ¹¹F. Aguilera-Granja, J. L. Rodríguez-López, K. Michaelian, E. O. Berlanga-Ramírez, and A. Vega, *Phys. Rev. B* **66**, 224410 (2002).
- ¹²R. A. Guirado-López, J. Dorantes-Davila, and G. M. Pastor, *Phys. Rev. Lett.* **90**, 226402 (2003).
- ¹³Y. Ch. Bae, H. Osanai, V. Kumar, and Y. Kawazoe, *Phys. Rev. B* **70**, 195413 (2004).
- ¹⁴L. Xiao and L. Wang, *J. Phys. Chem. A* **108**, 8605 (2004).
- ¹⁵D. A. Papaconstantopoulos, *Handbook of the Band Structure of Elemental Solids* (Plenum, New York, 1986).
- ¹⁶R. Haydock, *Solid State Physics*, edited by E. Ehrenreich, F. Seitz, and D. Turnbull, Vol. 35 (Academic Press, London, 1980), p. 215.
- ¹⁷C. Kittel, *Introduction to Solid State Physics*, 7th ed. (Wiley, New

York, 1996).

- ¹⁸J. L. Rodríguez-López, F. Aguilera-Granja, K. Michaelian, and A. Vega, *Phys. Rev. B* **67**, 174413 (2003).
- ¹⁹F. Aguilera-Granja, S. Bouarab, M. J. López, A. Vega, J. M. Montejano-Carrizales, M. P. Iñiguez, and J. A. Alonso, *Phys. Rev. B* **57**, 12469 (1998).
- ²⁰M. Moseler, H. Häkkinen, R. N. Barnett, and U. Landman, *Phys. Rev. Lett.* **86**, 2545 (2001).
- ²¹V. Kumar and Y. Kawazoe, *Phys. Rev. B* **66**, 144413 (2002); , *Eur. Phys. J. D* **24**, 81 (2003).
- ²²F. Aguilera-Granja, J. M. Montejano-Carrizales, and A. Vega, *Phys. Lett. A* **332**, 107 (2004); F. Aguilera-Granja, J. M. Montejano-Carrizales, E. O. Berlanga-Ramírez, and A. Vega, *ibid.* **330**, 126 (2004).
- ²³S. Baroni, A. Dal Corso, S. de Gironcoli, P. Giannozzi, C. Cavazzoni, G. Ballabio, S. Scandolo, G. Chiarotti, P. Focher, A. Pasquarello, K. Laasonen, A. Trave, R. Car, N. Marzari, and A. Kokalj, *Quantum ESPRESSO, opEn-Source Package for Research in Electronic Structure, Simulation, and Optimization*, <http://www.quantum-espresso.org/>
- ²⁴G. M. Pastor, J. Dorantes-Dávila, and K. H. Bennemann, *Phys. Rev. B* **40**, 7642 (1989).
- ²⁵Z. Q. Li and B. L. Gu, *Phys. Rev. B* **47**, 13611 (1993).
- ²⁶K. Miura, H. Kimura, and S. Imanaga, *Phys. Rev. B* **50**, 10335 (1994).
- ²⁷J. Guevara, F. Parisi, A. M. Llois, and M. Weissmann, *Phys. Rev. B* **55**, 13283 (1997).
- ²⁸A. N. Andriotis and M. Menon, *Phys. Rev. B* **57**, 10069 (1998).
- ²⁹E. O. Berlanga-Ramírez, F. Aguilera-Granja, A. Díaz-Ortiz, and A. Vega, *Eur. Phys. J. D* **23**, 343 (2003).
- ³⁰R. Guirado-López, P. Villaseñor-González, J. Dorantes-Dávila, and G. M. Pastor, *J. Appl. Phys.* **87**, 4906 (2000); R. Guirado-López, P. Villaseñor-González, J. Dorantes-Dávila, and G. M. Pastor, *Eur. Phys. J. D* **24**, 73 (2003).
- ³¹G. W. Zhang, Y. P. Feng, and C. K. Ong, *Phys. Rev. B* **54**, 17208 (1996).
- ³²B. V. Reddy, S. K. Nayak, S. N. Khanna, B. K. Rao, and P. Jena, *Phys. Rev. B* **59**, 5214 (1999).